Precipitation of gold into metastable gold silicide in silicon

Frieder H. Baumann* and Wolfgang Schröter
IV.Physikalisches Institut der Universität Göttingen and Sonderforschungsbereich 126 Göttingen/Clausthal, Bunsenstrasse 11-15, D-3400 Göttingen, Federal Republic of Germany
(Received 13 September 1990)

We report a detailed investigation of the precipitation behavior of gold in float-zone silicon from a highly supersaturated solution. Nucleation, morphology, and crystallography as well as the decomposition of the solution were examined using high-resolution electron microscopy, selected area diffraction combined with tilting experiments, Hall-effect measurements, and energy dispersive x-ray spectroscopy. After in-diffusion of gold at 1275 °C annealing experiments were performed at 850 °C for durations ranging from 5 min up to 35 d. It is shown that gold precipitates in small spherical particles (diameter: 10–20 nm) consisting of a metastable gold silicide. By means of selected area diffraction combined with a special tilting procedure, the unit cell is proved to be orthorhombic with lattice parameters $a=0.971$ nm, $b=0.768$ nm, and $c=0.703$ nm. Systematic absence of reflections in several precipitate zone-axis patterns reveals the space group of the silicide to be $Pnma$ or $Pn2_1a$. According to Hall-effect measurements the concentration of substitutional gold decreases to a few percent within 5 min annealing at 850 °C. Only a part of it has precipitated in gold silicide particles, which are found at small extrinsic stacking faults. The stacking faults represent a density of self-interstitials Si_i of about 10^{18} cm^{-3}, which according to control experiments is about a factor of 50 above the equilibrium concentration of Si_i at 1274 °C. As annealing proceeds the stacking faults disappear, and gold is finally found in spherical particles embedded stress-free into the silicon matrix.

I. INTRODUCTION

Precipitation from a supersaturated solution is characterized by (1) the final state, to which the solution proceeds, and (2) the path of the solution towards it. Under the conditions of normal supersaturation the final state is the thermodynamically stable phase and the path to it is by nucleation of this phase and growth of it. If the solution is highly supersaturated or open, a metastable phase with nonequilibrium shape, structure, or composition might occur and the path towards it certainly contributes to its selection. "Open solid solutions" have recently gained considerable interest, as, e.g., metallic solutions under particle irradiation[1] or semiconducting solutions under gettering conditions, i.e., injection of point defects.[2]

We confine ourselves here to silicon with transition elements in high supersaturation. The questions are, what principle determines the phase that is formed as opposed to other possible phases? Which phases are accessible to the relaxing solution? Bené[3] has recently conjectured that the selected phase is a compromise which allows the solution to realize a maximum rate of energy degradation. Although seemingly plausible, this conjecture still needs theoretical and experimental justification. It presumably also needs specification since metastability should be associated with a time scale.

It has been recently shown that the precipitation of transition elements in silicon can occur easily under the conditions of large supersaturation. This is due to the fact that the solubility of these elements is exponentially decreasing with inverse temperature with activation enthalpies between 1.5 and 2.1 eV.[4] After in-diffusion of Ni and rapid cooling (10^3 K s^{-1}) from high temperatures (850 °C–1050 °C) platelets consisting of two $NiSi_2$ {111} layers have been found.[5] In these precipitates all nickel atoms have a deficient coordination. Similar results have been obtained for Co in Si.[6,7] The authors[5] argue that, although the platelets exhibit a large surface energy in addition to the energy associated with a dislocation, bounding the platelet, the bounding dislocation might be the most efficient channel for the formation of $NiSi_2$. The thickness of the platelet then results from the fact that just two $NiSi_2$ stackings extend into the dislocation core and can grow via it. However, it is not possible to study nucleation and growth of these platelets in earlier stages, since Ni and Co, due to their high diffusivity, fully precipitate even during fastest quenching.

In this work we demonstrate that Si/Au is a system, which on relaxation from high supersaturation precipitates into a new metastable phase. The evolution of this phase with time occurs during annealing and therefore can be well controlled. Unlike the group-3d elements Ni and Co, Au dissolves mainly on substitutional sites, can be quenched in those sites, and precipitates during subsequent annealing. The phase diagram of Si/Au shows a simple eutectic and hence gold particles are expected from precipitation. Under the condition of large supersaturation ($[Au^{dissolved}]/[Au^{eq}]=100$, if quenched from 1275 °C and annealed at 850 °C), we observe the formation of particles of a gold silicide.

We have applied electron microscope techniques to determine the space group of this silicide. Part of these results have been reported previously.[8] New results con-

cerning the orientational relationship between particles and matrix as well as extinction systematics are given in Sec. III B; these results allow us to confine the possible space groups to *Pnma* or $Pn2_1a$. The main concern of this work is to investigate the nucleation and development of the gold silicide particles (Sec. III A). We find that the particles of this phase nucleate at extrinsic stacking faults and show a strong faceting along {111} planes of silicon. The origin of the stacking faults, occurring in a density far above that of a control sample, still growing in diameter during gold precipitation, and then strongly decreasing in number, must be caused by the in-diffusion of gold from the silicon surface, but is not understood at present. At the end of the precipitation period isolated particles of gold silicide without any electron microscopic indication of a stress field around them are seen. In the further development the particles lose faceting, become spherical, decrease in number, and increase in size.

II. EXPERIMENTAL PROCEDURE

Float-zone silicon (Wacker Chemitronic, 1.5×10^{16} B atoms/cm^3) was cut into rectangular samples ($2\times5\times10$ mm^3), which were polished, carefully cleaned, and etched in HF:HNO_3 (1:14). After evaporation of 17 nm of gold (purity 99.99%) the specimens were annealed in a quartz tube under Ar atmosphere at 1275 °C for 72 h to attain the solubility of substitutional gold, which is $[Au_s^{eq}]=1.6\times10^{17}$ cm^{-3}.[9] After quenching in ethylene glycol the residual eutectic was removed from the surface using aqua regia.

After another cleaning and etching procedure the specimens were annealed in a quartz tube under Ar atmosphere at 850 °C ($[Au_s^{eq}]=1\times10^{15}$ cm^{-3}), one for each of the following times: 5 min, 1 h, 4 h, 8 h, 1 d, 5 d, 17 d, and 35 d. Again annealing was finished by quenching the specimens into ethylene glycol (quenching rate $\approx10^3$ K s^{-1}).

For electron microscopic investigation the samples were mechanically thinned to about 10 μm and then thinned by ion milling (Ar, 2.5–4.5 kV).

High resolution transmission electron microscopy (HRTEM) investigations were performed in a Philips EM 420 ST operating at 120 kV and equipped with a double tilt specimen holder (±10°). Selected-area-diffraction patterns (SADP) of precipitates were calibrated using the silicon matrix spots and energy dispersive x-ray analysis was carried out in a Philips 400 T with a beryllium specimen holder.

Hall-effect data were obtained for a magnetic field of 0.579 T in a temperature range from 78 to 340 K using a lock-in technique. The hole concentration was calculated from the Hall coefficient R_H using the relation

$$p(T)=\frac{r_H}{R_H(T)e},$$

where e denotes the elementary charge. The Hall factor r_H was taken from the work of Messier and Flores.[10]

III. EXPERIMENTAL RESULTS

A. Kinetics and morphology of precipitation

1. Hall data

Figure 1 shows the hole density as a function of inverse temperature $p(1/T)$ for four samples. Curve 1 represents $p(1/T)$ for the starting material, curve 2 after in-diffusion of gold at 1275 °C for three days and quenching to room temperature. Obviously the material has become compensated by the substitutional species of gold, which is known to introduce a donor level at $E_V+0.35$ eV.[11] The slope of curve 2 yields this value as activation enthalpy.

Assuming an ionization entropy $S=3k_B$ (k_B is the Boltzmann constant),[12] one obtains from curve 2 the value of $[Au_s]=4.7\times10^{16}$ cm^{-3}, which is only about 30% of the gold solubility at this temperature: $[Au_s^{eq}]=1.6\times10^{17}$ cm^{-3}, as determined by neutron activation analysis (NAA).[9] There is evidence in the literature,[13,14] that in this range the gold concentration as derived from Hall data only gives a lower limit.

Curve 3 of Fig. 1 shows $p(1/T)$ of a sample saturated with gold at 1275 °C after additional annealing at 850 °C for 5 min. From the remaining electric compensation we obtain $[Au_s]=7\times10^{15}$ cm^{-3}, which corresponds to an annealed fraction of 0.85 referring to the initial value as derived from the Hall data and to 0.97 assuming that the

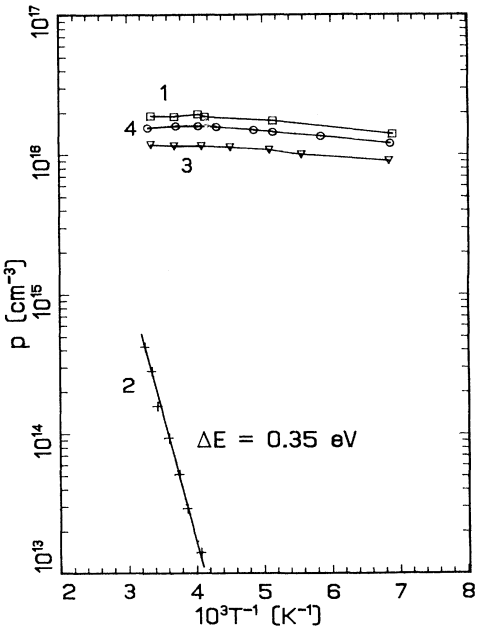

FIG. 1. Carrier concentration as measured by Hall effect for different stages of precipitation. 1, starting material. 2, after saturation with gold at 1275 °C for three days and quenching to room temperature. 3, after saturation at 1275 °C and 5 min annealing at 850 °C. 4, after annealing at 850 °C for 1 h. The slope of curve 2 corresponds to the activation enthalpy of the gold donor in silicon ($E_V+0.35$ eV).

solubility as derived from NAA (Ref. 9) has been reached during the in-diffusion. This time scale for the degradation of the gold donor agrees well with the extrapolation of recent results, which were obtained by deep level transient spectroscopy (DLTS) and Hall effect of Au in Si in the temperature range from 500 °C to 700 °C.[15]

After 1 h annealing at 850 °C curve 4 in Fig. 1 is measured. It yields a remaining concentration of gold donors of $[Au_s]=3\times10^{15}$ cm^{-3}, which—within the limits of error—agrees with the solubility of Au_s at 850 °C: $[Au_s(850\,°C)]=2\times10^{15}$ cm^{-3}.[9]

In conclusion, the degradation of the gold donor is already rather advanced after 5 min and completed in less than 1 h at 850 °C.

2. *Electron microscopic investigations*

a. Initial stage (after in-diffusion of gold). In the initial stage, i.e., after in-diffusion of gold at 1275 °C and quenching to room temperature, no defects at all were found by means of HRTEM and conventional electron microscopy (CTEM). If any agglomerates are present, their size is below the detection limit of TEM, which is about 2 nm. The Miller indices of the gold silicide, which are given below, refer to the orthorhombic phase described in Ref. 8 and in Sec. III B.

b. First stage of precipitation (850 °C, 5 min). Additional annealing at 850 °C for 5 min yields numerous small planar defects all over the specimen. The density of these defects has been evaluated from counting them in a steep wedge and estimating the volume of the wedge via the extinction contours on a two-beam bright-field micrograph. As a result we obtained $N_{plan}=3\times10^{13}$ cm^{-3}.

Some details of these defects can be seen from Fig. 2, which shows a HRTEM image of silicon in (110) orientation containing such planar defects (a), a SADP of the same region (b), and a slanted reproduction (c) of the lattice image in (a). As also proven by streaks in the SADP, the defect has a platelike shape with an extra (111) double plane [Fig. 2(c)] on silicon (111), and the diameter is about 50 nm.

The lattice image does not tell us whether the planar defect is an extrinsic stacking fault or planar gold precipitation. To answer this question we have estimated the concentration of atoms involved in the formation of these defects from their density, which is 3×10^{13} cm^{-3}, and their mean diameter, which is 56 nm as determined from 60 observed platelets. This concentration amounts to 1×10^{18} cm^{-3} atoms and exceeds the solubility of gold at diffusion temperature by a factor of about 6. We therefore conclude that the platelets are extrinsic stacking faults (Frank loops) resulting from the condensation of self-interstitials.

To further confirm this identification we have performed control experiments. Specimens from the same material and of the same dimensions were cleaned and etched, but not covered with gold. They have been etched in aqua regia, and the surfaces of one of them were additionally roughened with boron carbide (grain 1000). They were annealed at 1275 °C for 72 h, quenched to room temperature, cleaned, and then further annealed at 850 °C for 5 min to generate the stacking faults. Please note that under these boundary conditions the "equilibrium concentration" of silicon interstitial at 1275 °C should be adjusted within the crystal.

We find platelets which look identical to those observed after gold diffusion. From their density (3×10^{11} cm^{-3}) and mean diameter (112 nm) we estimate $[Si_i]=4\times10^{16}$ cm^{-3}. Within its margins of error this value is equal to the equilibrium concentration of silicon interstitials $[Si_i^{eq}]=2.4\times10^{16}$ cm^{-3}, as estimated by Tan and Gösele.[16] This agreement strongly supports our identification of the platelets as stacking faults. It also shows that with liquid gold-silicon eutectic on the surface the silicon interstitial concentration is significantly larger compared to that observed for an etched mechanically polished silicon surface.

Evidence that first gold agglomerates have formed is given by the two micrographs shown in Fig. 3. In Fig. 3(a) near to a Frank loop, which is imaged by an incident beam parallel to the ⟨110⟩ Si foil normal, a dark blob (arrow) is seen. In Fig. 3(b) the same defect is imaged with the specimen slightly tilted off the exact ⟨110⟩ Si

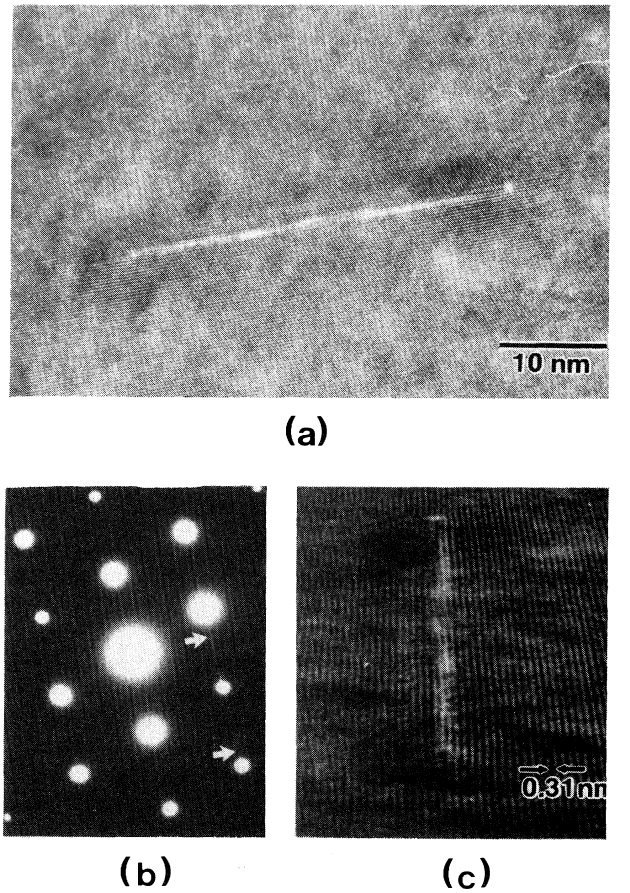

FIG. 2. $t_{ann}=5$ min. (a) Lattice image of a platelet parallel to $(111)_{Si}$ plane. (b) Streaks in the diffraction pattern show the planar nature of the defect. (c) Slanted reproduction of micrograph (a) illustrates that the plate consists of an additional (111) double plane.

orientation to reduce the strain contrast. In the region of the dark blob a strong amplitude contrast, which turned out to be independent on defocus, is now seen. Also the sharp faceting along the (111) Si planes indicates that the observed contrast originates from early stages of gold precipitation. The particle was too small to give rise to visible reflections in SADP. We have observed only this one example; all other observed platelets seem to be undecorated.

c. Second stage of precipitation (850 °C, 1–8 h). After 1 h annealing at 850 °C the density of platelets has decreased by an order of magnitude to about 2.5×10^{12} cm^{-3} with an almost unchanged mean diameter of 60 nm. A considerable fraction of the Frank loops has become decorated now. The diameter of the silicide particles lies between 6 and 12 nm.

As demonstrated in Fig. 4, the decoration results from small gold silicide precipitates. In Fig. 4(a) a platelike defect (arrows) together with a faceted particle is seen, whose diameter is about 15 nm and which generates visible reflections in the SAD mode. By tilting the specimen SADP's of low-index orientations of the silicide structure have been obtained. Figure 4(b) presents a lattice image of the same particle at the (111) silicide pole and also the corresponding SADP. The (110), (101), and (011) planes of the silicide structure are clearly resolved; their planar spacings are marked in the micrograph. The corresponding plane normals are indicated in the diffraction pattern and the periodicity of the precipitate reflections is illustrated by arrows in the right part of the pattern. Tilting the specimen around the [110] axis by 18.30° results in the (211) orientation [Fig. 4(c)], in which the (110) planes and the (111) planes are resolved.

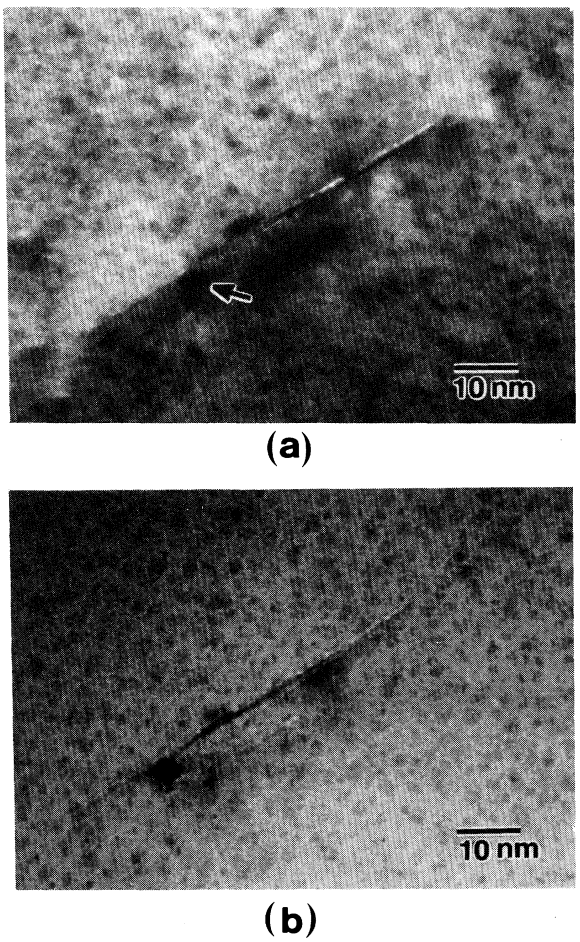

FIG. 3. $t_{ann}=8$ h. (a) HRTEM micrograph of a platelet with a dark blob (see arrow) in its very vicinity, incident beam exactly along $[110]_{Si}$. (b) Tilted illumination reduces strain contrast and shows the decoration of the platelet to produce distinct amplitude contrast. Note the sharp faceting of the particle which further indicates that the particle represents an early stage of precipitation.

After 4 h annealing the density of platelets has not changed (2.5×10^{12} cm^{-3}), but their mean diameter has increased to about 120 nm. With the exception of a few the platelets are decorated, but also isolated precipitates are observed (see, e.g., Fig. 11). Their diameter lies between 10 and 18 nm.

After 8 h annealing the Frank loops have slightly increased in density to 5×10^{12} cm^{-3} and mean diameter to 130 nm. Silicide particles are found isolated [Fig. 10(a)] or at large platelets [Fig. 5(a)]; their diameter has not changed. In one case two silicide particles are observed at the same platelet [Fig. 5(b)].

d. Final stage of precipitation (850 °C, 1–35 d). At the beginning of this stage the platelets have disappeared and the silicide particles apparently have a rather weak strain field around them, since they cannot be detected by means of CTEM, but only by scanning the sample at rather high resolution. Therefore it was not possible to determine the density of the precipitates even roughly. The precipitates, which are found after annealing for 1 d, exhibit strong faceting along the (111) Si planes (see Fig. 6). Both micrographs were recorded in (110) orientation of the silicon matrix. Please note that the periodic pattern inside the particles has to be interpreted as Moiré contrast and does not represent a lattice image of the silicide structure.

Faceting is an intermediate state in the development of the particles. After 5 d annealing it is almost lost. More spherical particles are found now, as can be seen in Fig. 7 [lattice image along the (212) zone axis of the silicide structure]. Some faint traces of faceting, however, remain visible even after 17 d annealing. Figure 8(a), a HRTEM micrograph in (110) orientation of the silicon matrix, shows an example. Figure 8(b), taken for the same orientation, shows another interesting feature: The two particles imaged are 100 nm apart and have a diameter above the mean diameter, which remains unchanged. For the particle in the lower left a clear variation of the Moiré contrast can be seen, which indicates lattice defects inside the precipitate.

The crystal structure of the gold silicide apparently remains unchanged, even after 35 d of annealing. The HRTEM picture of a precipitate along the (278) zone axis of the silicide (Fig. 9) shows the spacings, which corresponds to the (122) planes (0.250 nm), the (321) planes (0.233 nm), and the (401) planes (0.229 nm).

In conclusion, we have observed by HRTEM two types of defects—extrinsic stacking faults and gold silicide particles—whose nucleation and development are strongly locally and apparently also temporarily correlated. At the final stage we are left with small spherical gold silicide particles, which are metastable in structure and are embedded stress-free into the silicon matrix.

B. Space group of the gold silicide precipitates

First results, showing that the precipitates contain gold and that their unit cell is orthorhombic with $a=0.96$ nm, $b=0.77$ nm, and $c=0.69$ nm, have been published previously.[8] In the meantime we have obtained new results, which give more precise lattice constants, and allow one

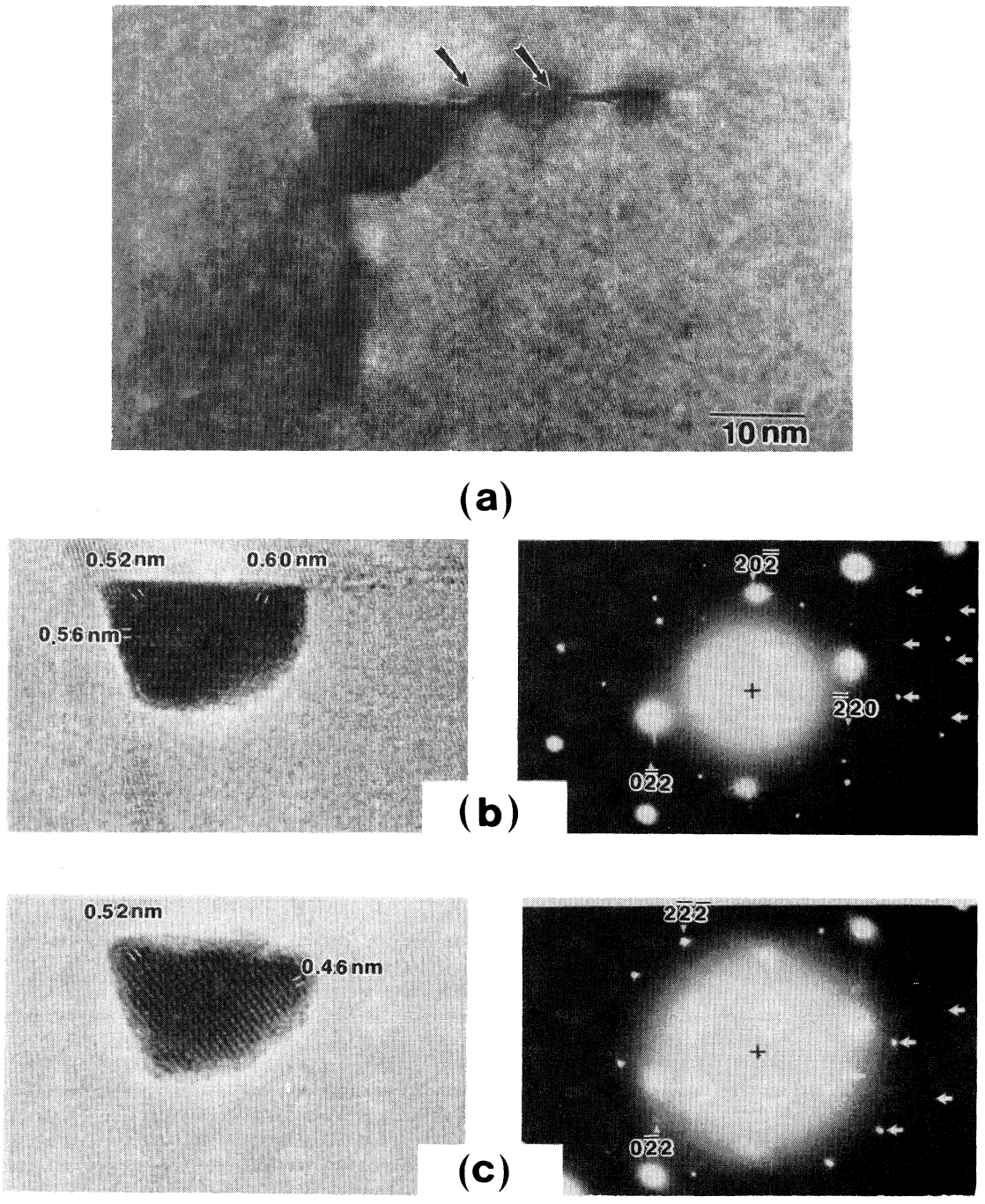

FIG. 4. $t_{ann}=8$h. (a) HRTEM micrograph of a gold silicide precipitate decorating a platelet (arrows) in the silicon matrix, electron beam along $[110]_{Si}$. (b) Lattice image of the same precipitate at the (111) silicide pole. In the corresponding SAPD some silicide reflections are denoted and the periodicity of the silicide reflexes is illustrated by arrows. (c) Same precipitate imaged in (211) orientation after the specimen was tilted around the [110] axis of the silicide by an angle of 18.3°.

to define closely the possible space group and to state additional extinction rules.

As a result of a fitting procedure to about 40 low-index SADP's the lattice constants of the orthorhombic unit cell are determined with higher accuracy now: $a=0.971\pm0.005$ nm, $b=0.768\pm0.005$ nm, and $c=0.703\pm0.005$ nm. As already indicated previously, $b=\sqrt{2}a_{Si}=0.7679$ indicates coherence between precipitates and silicon matrix in ⟨110⟩ Si direction. In fact, all precipitates were found to obey this orientational relationship between (001) silicide and (110) Si.

The symmetry of the gold silicide unit cell, i.e., its space group, was determined by collecting the systematic extinctions observed in low-index orientations of the precipitates. First evidence of systematic extinctions is given in a previous paper,[8] where the absence of odd numbered reflections in all fundamental periods was shown.

Figure 10(a) is a HRTEM micrograph of a precipitate [$t_{ann}(850\,°C)=8$ h] in (010) silicide orientation; Fig. 10(b) shows the corresponding SADP. The absence of reflections (001), (003), as well as (500) indicate extinctions in the unit-cell periods for uneven indices [see also Figs. 12(a)–12(c)]. Note the simultaneous orientation of matrix (110) and precipitate (010), which supports once again the orientation relationship mentioned above.

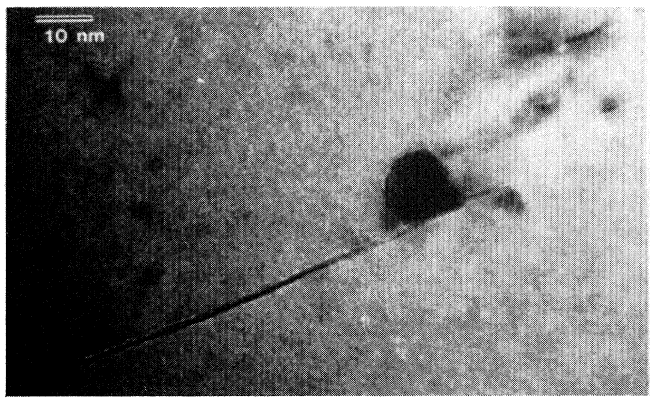

(a)

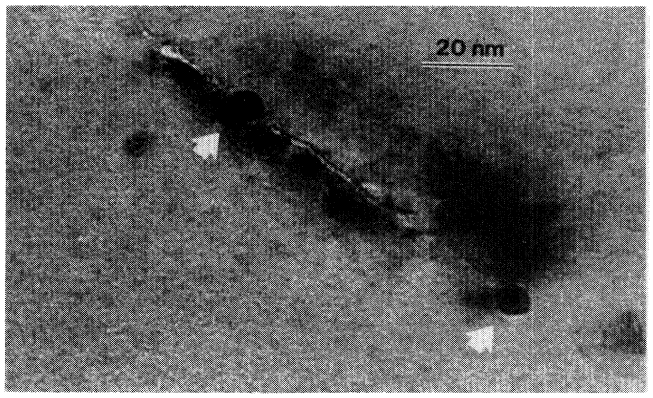

(b)

FIG. 5. $t_{ann}=8$h. (a) Large planar defect on a $(111)_{Si}$ plane decorated by a silicide precipitate. the grid inside the particle occurs due to Moiré contrast. (b) Bright-field micrograph of *two* precipitates formed at a single planar defect.

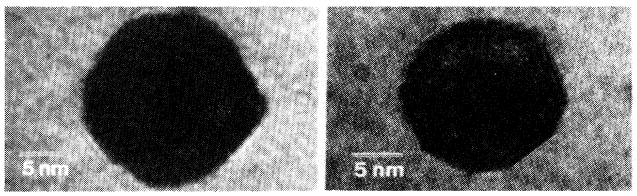

FIG. 6. $t_{ann}=1$ d. Precipitates found after 1 d annealing exhibit strong faceting along the $(111)_{Si}$ planes.

So far, the observed systematic extinction for uneven indices in all unit-cell periods reduce the number of possible space groups from 59 down to 31, since at least three screw axes are determined.

The existence of a zonal extinction rule is presented in Fig. 11. The HRTEM micrograph shows a precipitate [$t_{ann}(850\,°C)=4$ h] in (001) orientation. The SADP [Fig. 11(b)] reveals absence of all reflections of the type $hk0$ where h is odd. The symmetry of the unit cell therefore includes an axial glide plane with glide vector $a/2$. The right indexing of this pattern was checked additionally by tilting the precipitate in its (107) and (015) orientations by an amount of 11° and 12°, respectively.

Now only 11 space groups in the orthorhombic system are left which comply with the observed extinction rules: *Pnna*, *Pbca*, *Pnma*, *Pbna*, $Pn2_1a$, *Pnaa*, $B22_12$, *Bbm*2, *Bbmma*, *Bba*2, and *Bbcm*.

The next step in deducing the right space group consists of ascertaining that there are *no* extinctions for reflections of the type $h0l$, as indicated by Fig. 10(b) (i.e., the [010] SADP). Any extinction rule [$I(h0l)=0$ for $h+l$ odd, $I(h0l)=0$ for h odd, or $I(h0l)=0$ for l odd] would lead in Fig. 10(b) to the absence of rows of reflections, which could not be excited by double diffraction either. The occurrence of the reflections of the type $h0l$ was also shown in previously published SADP's.[8]

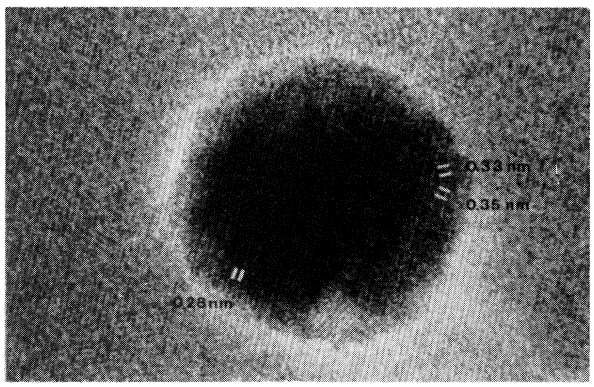

FIG. 7. $t_{ann}=5$ d. Lattice image of a spherical silicide particle in (212) orientation. The (021) planes (0.33 nm), the (120) planes (0.135 nm), and the (202) planes are resolved.

The only two space groups left fulfilling this additional condition (*no* extinctions for $h0l$) are the space groups $Pnma$ or D_{2h}^{16} and $Pn2_1a$ or C_{2v}^{9}, which have the following conditions limiting possible reflections: hkl, no limitations; $0kl$, $k+l=2n$; $h0l$, no limitations; $hk0$, $h=2n$; $h00$, $(h=2n)$; $0k0$, $(k=2n)$; and $00l$, $(l=2n)$.

These space groups, however, include a (100) glide plane with glide vector $(b+c)/2$, which restricts the occurrence of the $0kl$ reflections to $I(0kl)=0$ for $k+l$ odd. In fact, this additional extinction rule can be verified strictly only at the (100) silicide pole, which we did not succeed in observing. Nevertheless, Fig. 12 gives a strong hint to the required extinctions: Three SADP's of a single precipitate [$t_{ann}(850\,°C)=4$ h] are shown, tilted around the (100) axis towards each other by $\alpha_{ab}=+7.65°$ and $\alpha_{ac}=+18.3°$. Note the occurrence of the (011) reflection [Fig. 12(a)], while the (034) reflection and the

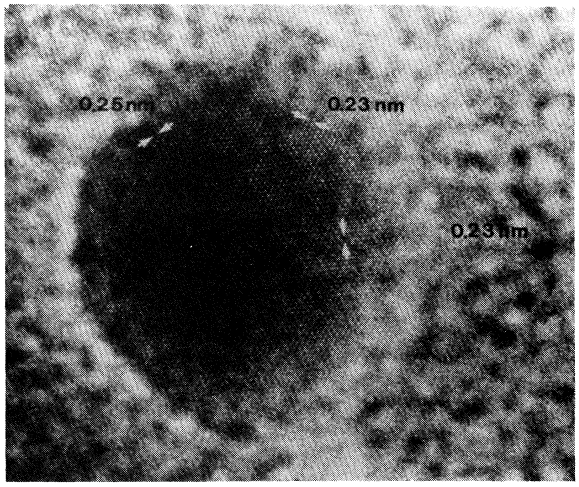

FIG. 9. $t_{ann}=35$ d. HRTEM micrograph of silicide particle imaged along the ⟨278⟩ zone axis. The (122), (321), and the (401) planes are resolved.

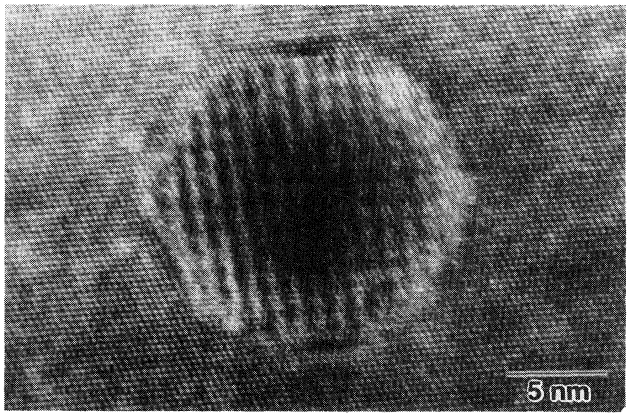

(a)

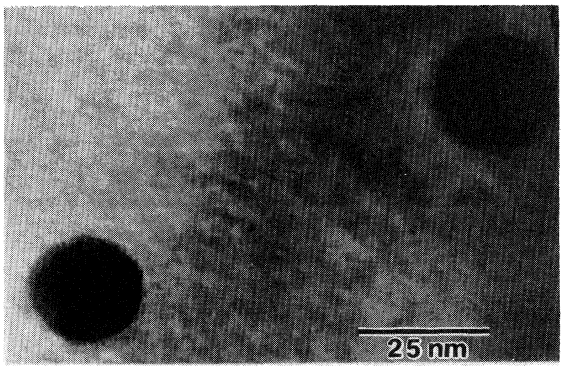

(b)

FIG. 8. $t_{ann}=17$ d. After long annealing times silicide precipitates are found to be perfectly spherical. (a) HRTEM micrograph of a spherical precipitate recorded at the [110] silicon zone axis. (b) Medium magnification HRTEM micrograph of *two* precipitates in close vicinity of less than 150 nm. The variation of Moiré contrast in the left-hand particle indicates the existence of defects *inside* the silicide precipitate.

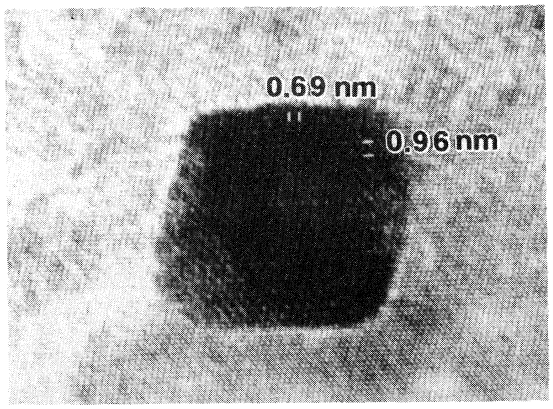

(a)

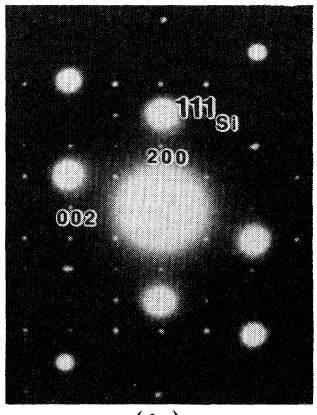

(b)

FIG. 10. $t_{ann}=8$ h. (a) Lattice image of a silicide precipitate in (010) orientation. Silicon matrix orientation is exactly [110], radius of objective aperture $r_{ap}=(0.17\text{ nm})^{-1}$. (b) SADP of the same precipitate. The rectangular pattern of small spots represents the [010] zone-axis pattern of the silicide. Note the absence of reflections in the unit-cell periods.

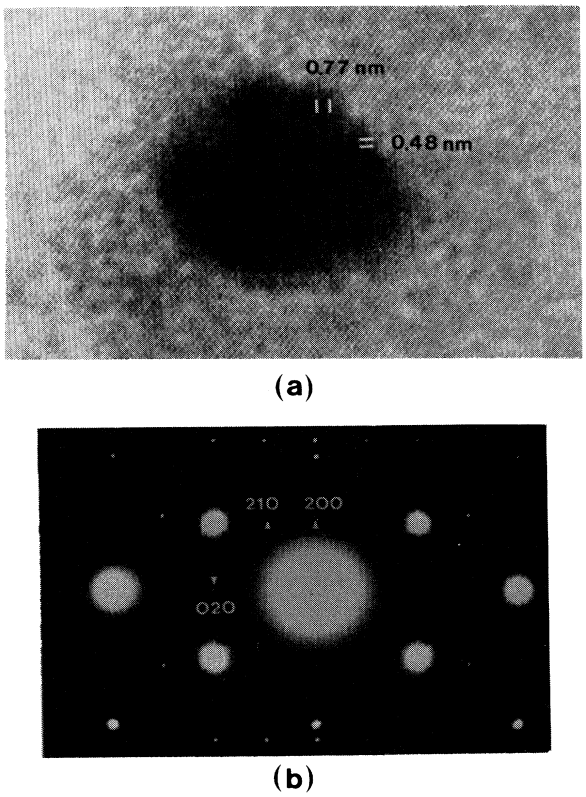

FIG. 11. $t_{ann}=4$ h. (a) HRTEM micrograph of a precipitate in (001) orientation of the silicide [$r_{ap}=(0.17\ \text{nm})^{-1}$]. The silicon matrix orientation is slightly off the [110] direction. (b) SADP of the same precipitate at the [001] pole, revealing the absence of all reflections of the type $hk0$ with h odd.

(012) reflection do *not* occur [see Figs. 12(b) and 12(c)]. This observation supports precisely the demanded extinction rule $I(0kl)=0$ for $k+l$ odd to be valid in our structure. It seems very reasonable therefore to assume that the symmetry of the gold silicide structure is represented either by the space group *Pnma* or $Pn2_1a$.

C. Energy dispersive x-ray analysis

Energy dispersive x-ray analysis was performed in a conventional TEM using a specimen holder equipped with a Be capsule. The electron beam (spot size: about 20 nm) was focused directly on a particle which formed after 8 h annealing at 850 °C; see, for example, Fig. 10(a) or 10(b). The diameter of the precipitate was approximately 15 nm. During the time of measurement (1000 sec) care was taken that the beam was focused on the precipitate all the time.

Except gold and silicon no additional elements were detected. However, since the precipitates are embedded in the silicon matrix, it is not possible to perform a quantitative analysis to determine the amount of gold inside the particle. Nevertheless, the absence of lines from other elements except gold strongly implies that the precipitates consist of a genuine gold silicide.

IV. DISCUSSION

During the relaxation of a supersaturated solution of gold in silicon at 850 °C we have found by means of HRTEM and selected area diffraction the formation of metastable gold silicide particles. A gold silicide is not existent as an equilibrium phase.

The formation of the Au_xSi_y particles (diameter 6–15 nm) is preceded or accompanied by the formation of stacking faults, whose density results from the precipitation of about 10^{18} Si_i per cm^3. This value exceeds the gold concentration in our specimen [Au^{eq}(1275 °C)] by a

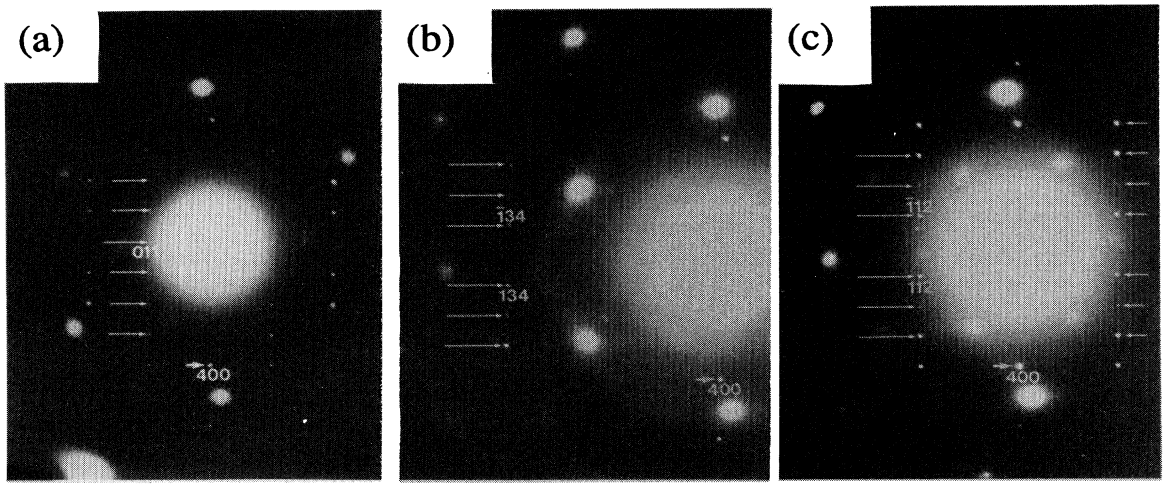

FIG. 12. $t_{ann}=4$ h. Three SADP's of a single precipitate rotated around the [100] direction of the silicide structure. (a) [011] zone-axis pattern, note the occurrence of the (011) reflections. (b) [043] zone-axis pattern, reflection (034) is absent. (c) [021] zone-axis pattern, reflection (012) is absent.

factor of about 6 and the "equilibrium concentration" of silicon interstitials, as found in a control experiment with no gold on the silicon surface, by more than one order of magnitude.

Apparently the presence of the gold-silicon eutectic on the silicon surface leads to a strong enhancement of the silicon interstitial concentration inside the specimen. Since until now the interpretation of gold diffusion experiments has been based on the assumption that the point defect equilibria are not affected by the liquid eutectic coverage, our results presumably require a reinterpretation of those results.

The estimate for $[Si_i^{eq}(1548\ K)] \approx 4\times10^{16}\ cm^{-3}$ from our control experiment agrees within its limit of margin with the value of $2.4\times10^{16}\ cm^{-3}$ given by Tan and Gösele.[16] It disagrees with estimates by Taniguchi *et al.*[17] ($1.3\times10^{17}\ cm^{-3}$) and by Bronner and Plummer ($1.0\times10^{15}\ cm^{-3}$).[18]

The nucleation and development of the Au_xSi_y particles can be only sketched because of the few available time intervals of annealing. The particles nucleate at the stacking faults and become visible by HRTEM occasionally after 5 min, generally after 1 h. Their mean diameter increases between 1 and 4 h and then stays almost constant. Up to 840 h we have not found any Oswald ripening and also no decomposition of the silicide into the eutectic. The observed changes concern the silicide-silicon interface, the defect structure inside the particles, and the stacking faults.

Obviously the stacking faults, whose density decreases by an order of magnitude between 5 min and 1 h, grow in diameter then (4 and 8 h) to compensate for the volume change induced by the gold precipitation. After 1 d of annealing the stacking faults have disappeared and leave behind isolated Au_xSi_y particles, which are embedded stress-free into the silicon matrix.

As the annealing time is increased from 1 to 4 h, the stacking fault diameter increases from 56 to 130 nm. This corresponds to the absorption of about 5×10^{17} Si_i per cm^3. We now show that the precipitation of about 1.6×10^{17} Au atoms per cm^3 can generate this concentration of Si_i. The silicide unit cell is 3.3 times that of Si in volume (0.524 nm^3 compared to 0.158 nm^3), and contains eight formula units of Au_xSi_y. The generation of an orthorhombic silicide unit cell thus produces $(26.5-8y)$ Si_i atoms. Assuming $x=2$ and $y=1$, precipitation of 1.6×10^{17} Au atoms into 10^{16} silicide unit cells produces 2×10^{17} Si_i atoms, which is close to our experimental value of 5×10^{17} Si_i per cm^3. Again with $x=2$ and $y=1$, 1.6×10^{17} Au atoms per cm^3 can be used to decorate each stacking fault with a single precipitate 16 nm in diameter. This value is also close to the precipitate diameter we observe in our experiments.

The nucleation of the Au_xSi_y particles is preceded by the concentration decrease of the gold donor according to the Hall measurements, i.e., by the disappearance of substitutional gold. It is unclear in which state gold exists after 5 min of annealing. Possibly it has drifted with the silicon interstitials and has concentrated around the stacking faults as a Cottrell cloud.

The unit cell of the metastable gold silicide was shown to be orthorhombic previously,[8] which allows one to index all the observed SADP's. By carefully analyzing the observed extinctions in the SADP's of several precipitates we are able to confine the unit-cell symmetry to *Pnma* or $Pn2_1a$. A further distinction between these two space groups cannot be made by means of selected area diffraction. However, to the knowledge of the authors this is the first time the unit cell of a gold silicide has been achieved unambiguously and its symmetry has been confined to only two possible space groups. Except for one proposition[19] there is no match with the various gold silicide structures reported in the literature.[20]

Though we find all precipitates to be aligned according to $[010]_{silicide}$ parallel to $[110]_{Si}$, we were not able to find a second relationship of coherence between silicide and matrix. In fact, while Fig. 10 indicates the $[100]_{silicide}$ direction to be almost parallel to $[111]_{Si}$, Fig. 11 shows the $[100]_{silicide}$ direction to be a few degrees off $[100]_{Si}$, and Fig. 12 finds the $[100]_{silicide}$ a few degrees off $[220]_{Si}$.

Concerning the path which determines the formation of a metastable structure, the interfacial energy between precipitate and matrix does not seem to be the only crucial parameter. This conclusion is supported by the fact that we found the same gold silicide after annealing (850 °C) and quenching a Au/Si multilayer stack. In the latter case the silicide was not surrounded by the silicon matrix forcing the silicide to obtain the orthorhombic structure. In addition, the various orientational relationships [except for the $(010)_{silicide}$ planes] indicate a rather loose coupling of matrix and precipitate.

However, a final answer to the question of the role of the interfacial energy can be given only after the composition of the Au_xSi_y compound and the positions of the atoms inside the unit cell have been determined.

ACKNOWLEDGMENTS

We would like to acknowledge M. Seibt and H. Feichtinger for helpful discussions and Professor P. Haasen, Institut für Metallphysik der Universität Göttingen, for laboratory facilities.

*Present address: AT&T Bell Laboratories, Crawford Corner Road, Holmdel, NJ, 07733.

[1]J. L. Bocquet and G. Martin, J. Nucl. Mater. **83**, 186 (1979).
[2]W. Schröter and R. Kühnapfel, Appl. Phys. Lett. **56**, 2207 (1990).
[3]R. W. Bené, J. Appl. Phys. **61**, 1826 (1987).
[4]E. R. Weber, Appl. Phys. A **30**, 1 (1983).
[5]M. Seibt and W. Schröter, Philos. Mag. A **59**, 337 (1989).
[6]J. Utzig, J. Appl. Phys. **64**, 3629 (1988).
[7]R. Kühnapfel, Ph.D. thesis, University of Göttingen, 1990 (unpublished).
[8]F. H. Baumann and W. Schröter, Philos. Mag. Lett. **57**, 75 (1988).
[9]N. A. Stolwijk, B. Schuster, J. Hölzl, H. Mehrer, and W.

Frank, Physica **116B**, 335 (1983).
[10]J. Messier and J. M. Flores, J. Phys. Chem. Solids **24**, 1539 (1963).
[11]A. G. Milnes, *Deep Impurities in Semiconductors* (Wiley, New York, 1973).
[12]R. Kassing, L. Cohaus, P. van Staa, W. Mackert, and H. J. Hoffmann, Appl. Phys. A **34**, 41 (1984).
[13]B. Brückner, Phys. Status Solidi A **4**, 1826 (1987).
[14]W. R. Thurber, D. L. Lewis, and W. M. Bullis, Air Force Cambridge Research Laboratories Report No. AFCRL-TR-73-0107, 1973 (unpublished).
[15]M. Morooka, H. Tomokage, and M. Yoshida, Jpn. J. Appl. Phys. **25**, 1161 (1986).
[16]T. Y. Tan and U. Gösele, Appl. Phys. A **37**, 1 (1985).
[17]K. Taniguchi, D. A. Antoniadis, and Y. Matsushita, Appl. Phys. Lett. **42**, 961 (1983).
[18]G. B. Bronner and J. D. Plummer, J. Appl. Phys. **61**, 5286 (1987).
[19]H. L. Gaigher and N. G. van der Berg, Thin Solid Films **68**, 373 (1985).
[20]H. Okamoto and T. B. Massalski, Bull. Alloy Phase Diagrams **4**, 190 (1983).

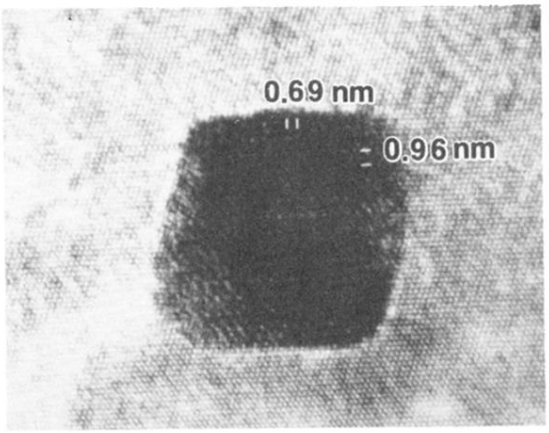

(a)

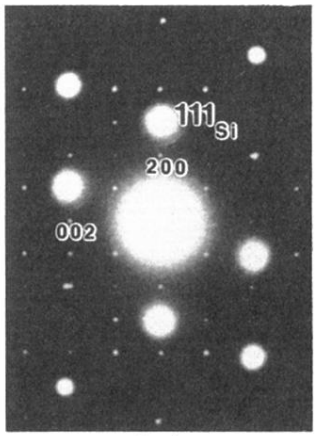

(b)

FIG. 10. $t_{ann} = 8$ h. (a) Lattice image of a silicide precipitate in (010) orientation. Silicon matrix orientation is exactly [110], radius of objective aperture $r_{ap} = (0.17\ \text{nm})^{-1}$. (b) SADP of the same precipitate. The rectangular pattern of small spots represents the [010] zone-axis pattern of the silicide. Note the absence of reflections in the unit-cell periods.

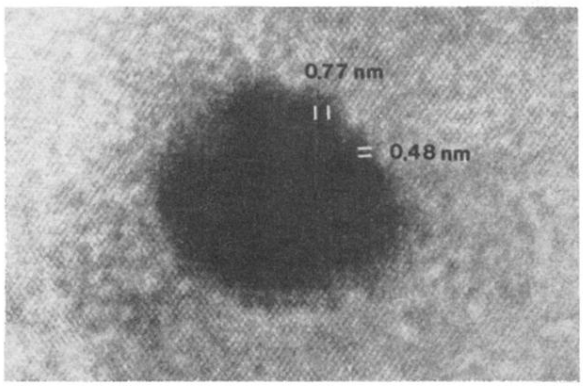

(a)

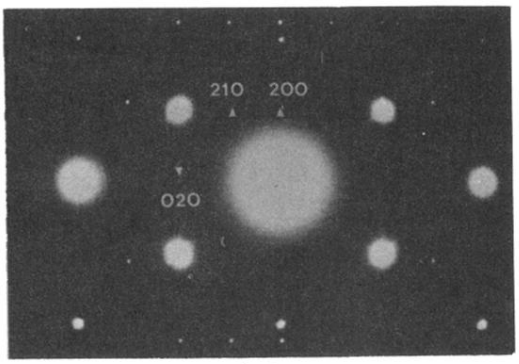

(b)

FIG. 11. $t_{ann}=4$ h. (a) HRTEM micrograph of a precipitate in (001) orientation of the silicide [$r_{ap}=(0.17\ \text{nm})^{-1}$]. The silicon matrix orientation is slightly off the [110] direction. (b) SADP of the same precipitate at the [001] pole, revealing the absence of all reflections of the type $hk0$ with h odd.

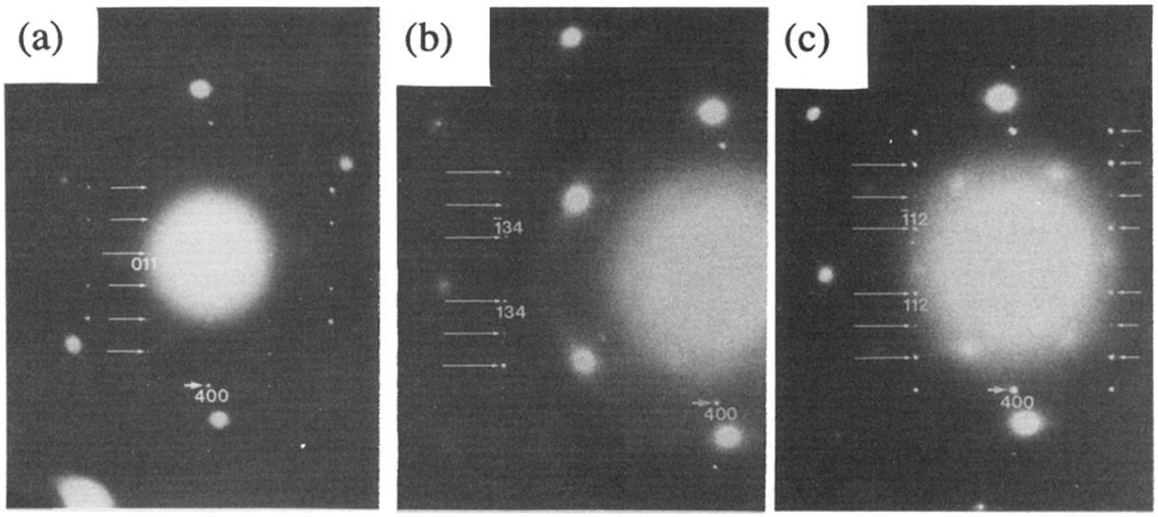

FIG. 12. $t_{ann}=4$ h. Three SADP's of a single precipitate rotated around the [100] direction of the silicide structure. (a) [011] zone-axis pattern, note the occurrence of the (011) reflections. (b) [043] zone-axis pattern, reflection (034) is absent. (c) [021] zone-axis pattern, reflection (012) is absent.

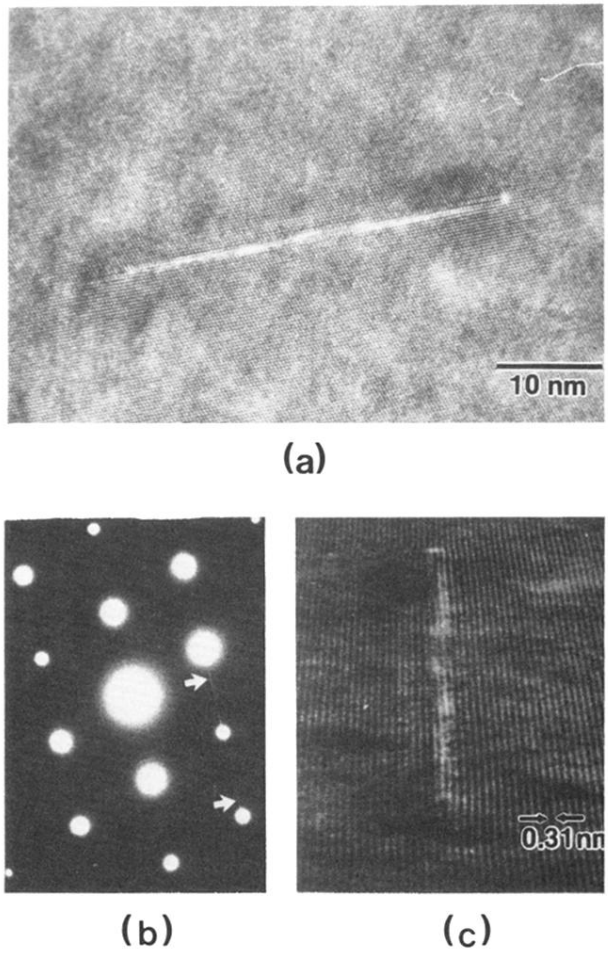

FIG. 2. $t_{ann} = 5$ min. (a) Lattice image of a platelet parallel to $(111)_{Si}$ plane. (b) Streaks in the diffraction pattern show the planar nature of the defect. (c) Slanted reproduction of micrograph (a) illustrates that the plate consists of an additional (111) double plane.

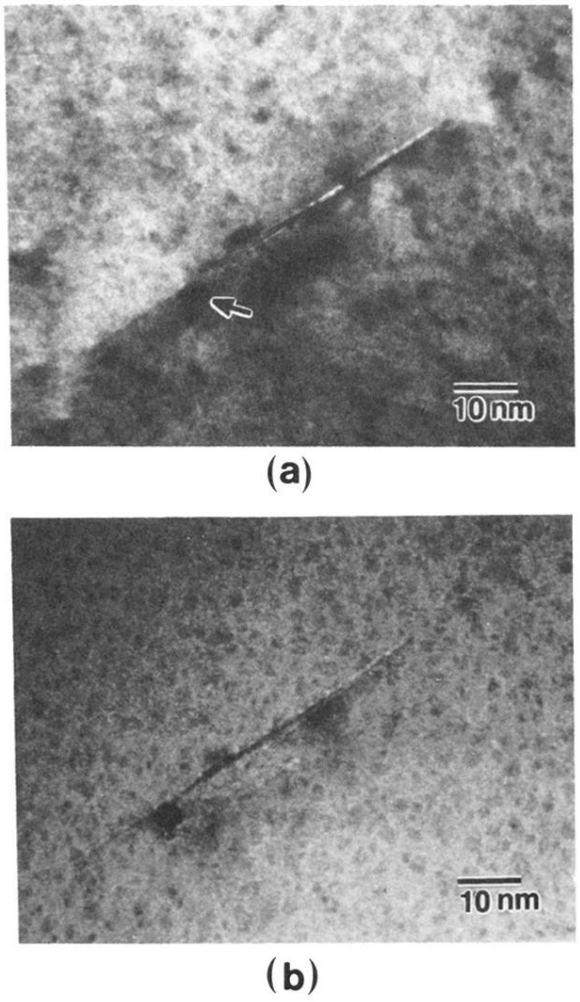

FIG. 3. $t_{ann} = 8$ h. (a) HRTEM micrograph of a platelet with a dark blob (see arrow) in its very vicinity, incident beam exactly along $[110]_{Si}$. (b) Tilted illumination reduces strain contrast and shows the decoration of the platelet to produce distinct amplitude contrast. Note the sharp faceting of the particle which further indicates that the particle represents an early stage of precipitation.

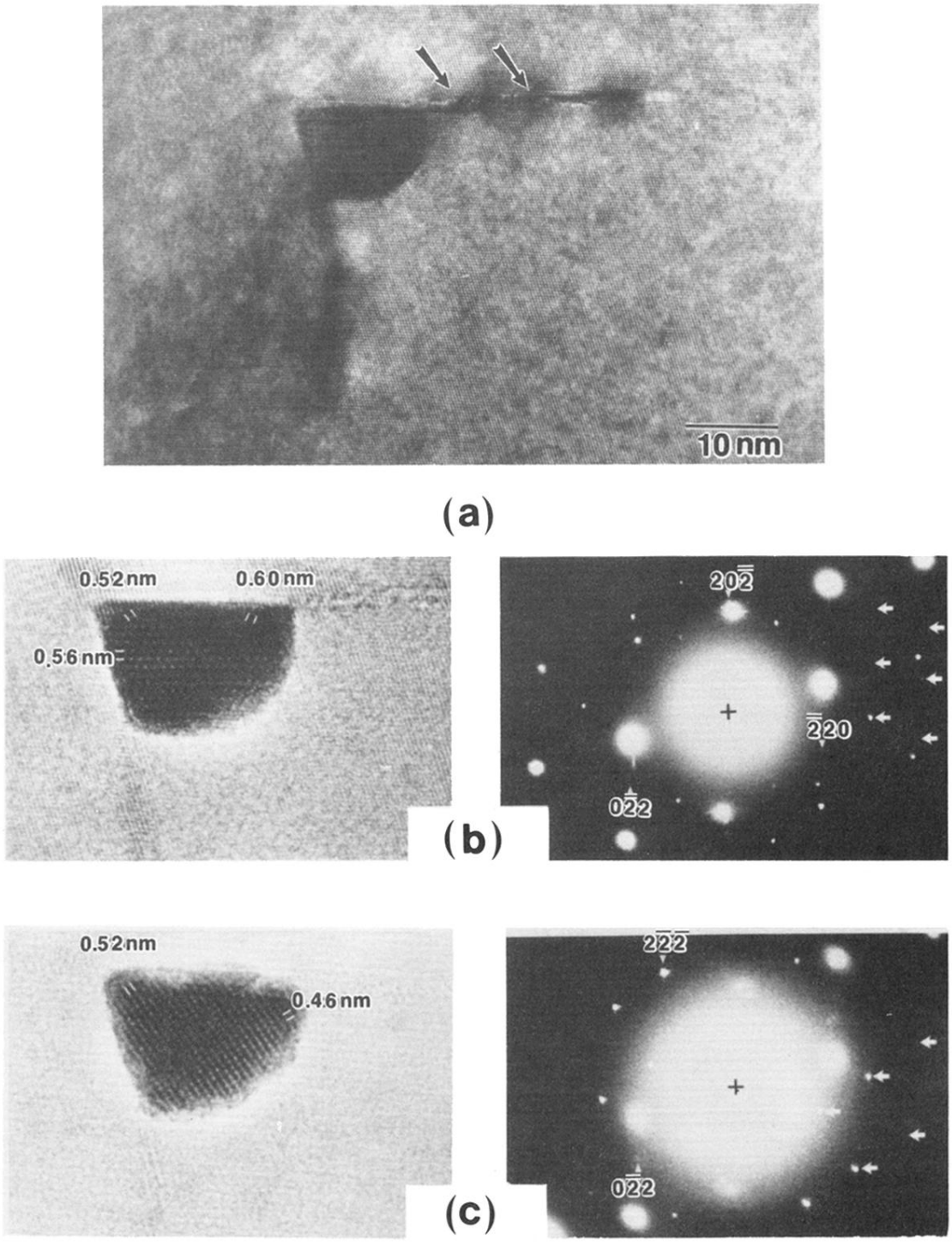

FIG. 4. $t_{ann} = 8h$. (a) HRTEM micrograph of a gold silicide precipitate decorating a platelet (arrows) in the silicon matrix, electron beam along $[110]_{Si}$. (b) Lattice image of the same precipitate at the (111) silicide pole. In the corresponding SAPD some silicide reflections are denoted and the periodicity of the silicide reflexes is illustrated by arrows. (c) Same precipitate imaged in (211) orientation after the specimen was tilted around the [110] axis of the silicide by an angle of 18.3°.

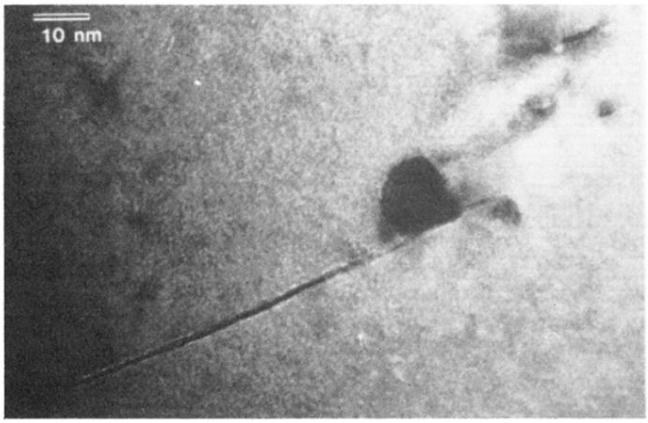

(a)

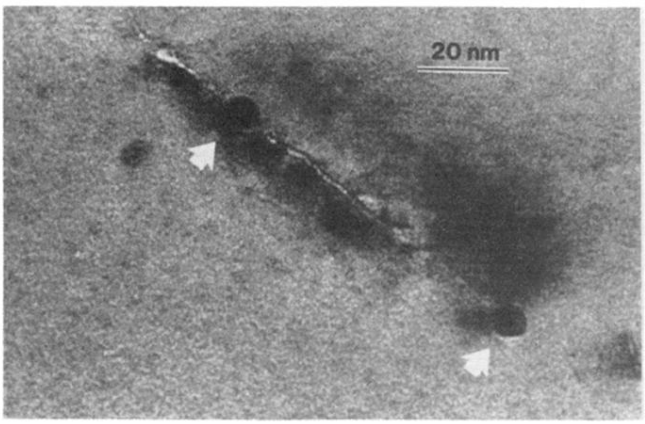

(b)

FIG. 5. $t_{ann}=8$h. (a) Large planar defect on a $(111)_{Si}$ plane decorated by a silicide precipitate. the grid inside the particle occurs due to Moiré contrast. (b) Bright-field micrograph of *two* precipitates formed at a single planar defect.

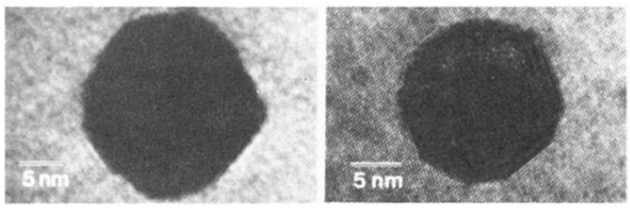

FIG. 6. $t_{ann} = 1$ d. Precipitates found after 1 d annealing exhibit strong faceting along the $(111)_{Si}$ planes.

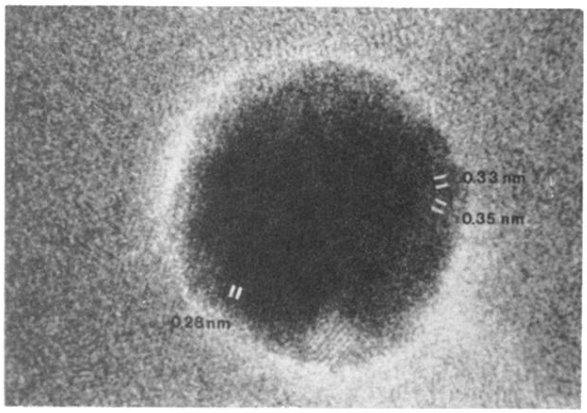

FIG. 7. $t_{ann} = 5$ d. Lattice image of a spherical silicide particle in (212) orientation. The (021) planes (0.33 nm), the (120) planes (0.135 nm), and the (202) planes are resolved.

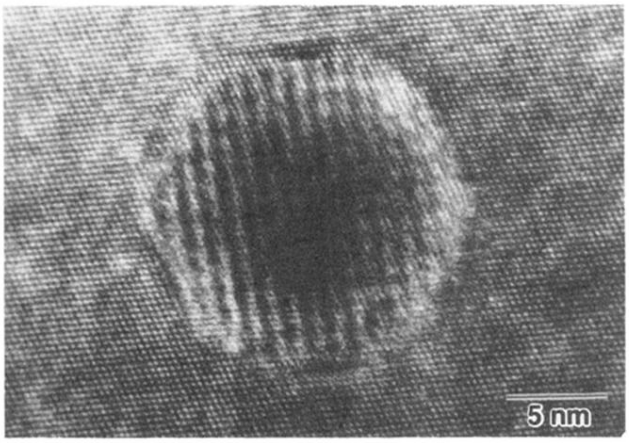

(a)

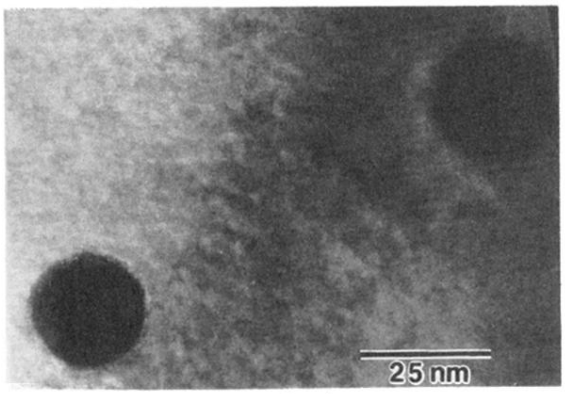

(b)

FIG. 8. $t_{ann} = 17$ d. After long annealing times silicide precipitates are found to be perfectly spherical. (a) HRTEM micrograph of a spherical precipitate recorded at the [110] silicon zone axis. (b) Medium magnification HRTEM micrograph of *two* precipitates in close vicinity of less than 150 nm. The variation of Moiré contrast in the left-hand particle indicates the existence of defects *inside* the silicide precipitate.

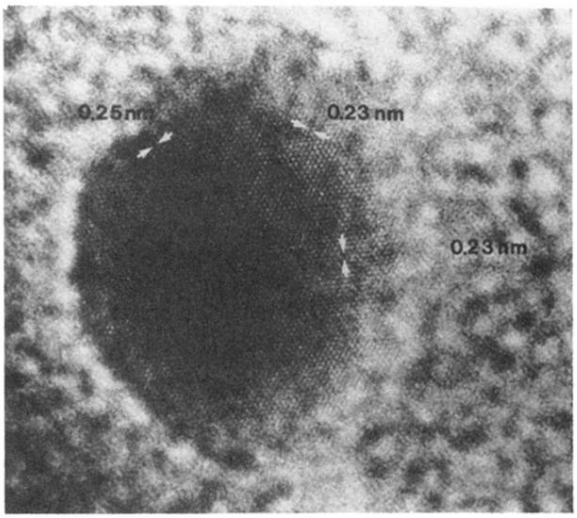

FIG. 9. $t_{ann} = 35$ d. HRTEM micrograph of silicide particle imaged along the ⟨278⟩ zone axis. The (122), (321), and the (401) planes are resolved.